Numerical simulation of the Gulf Stream System: The Loop Current and the deep circulation

Hyun-Chul Lee and George L. Mellor

Atmospheric and Oceanic Sciences Program, Princeton University, Princeton, New Jersey, USA

Received 23 July 2001; revised 2 August 2002; accepted 12 September 2002; published 21 February 2003.

[1] The Loop Current and the deep circulation in the Gulf of Mexico are numerically investigated by a primitive equation, sigma coordinate ocean model with realistic surface fluxes obtained from an atmospheric forecast model. A deep cyclonic circulation, bounded by the deep basin in the eastern Gulf of Mexico, is spun up by the Loop Current; the deep cyclonic circulation is coincident with a southward current of the Loop Current eastern limb and weakens after Loop Current ring separation and cessation of the southward current. The anticyclonic, semienclosed Loop Current also induces anticyclonic lower layer columnar eddies in the eastern gulf. These lower layer eddies decouple from the upper layer Loop Current. The westward translation speed of a Loop Current ring is about 2.16–5.18 km d^{-1}; the lower layer eddies have a higher speed and lead the rings into the central gulf. The time-averaged surface circulation of the Gulf of Mexico basin is anticyclonic, mainly because of the transport of anticyclonic vorticity by Loop Current rings in the surface layer an average lower layer cyclonic circulation occurs along the continental slope of the basin. *INDEX TERMS:* 4255 Oceanography: General: Numerical modeling; 4512 Oceanography: Physical: Currents; 4520 Oceanography: Physical: Eddies and mesoscale processes; 4243 Oceanography: General: Marginal and semienclosed seas; *KEYWORDS:* numerical modeling, Loop Current, deep circulation

Citation: Lee, H.-C., and G. L. Mellor, Numerical simulation of the Gulf Stream System: The Loop Current and the deep circulation, *J. Geophys. Res.*, *108*(C2), 3043, doi:10.1029/2001JC001074, 2003.

1. Introduction

[2] The Gulf of Mexico is a semienclosed sea with a basin deeper than 3500m. The circulation of the eastern Gulf of Mexico is dominated by the Loop Current which flows from the Yucatan Strait, then into the Strait of Florida after which it is called the Gulf Stream. Observational and theoretical studies describe how warm eddies shed from the Loop Current, translate across the gulf and collide against the continental slope of the western gulf [*Elliott*, 1982; *Kirwan et al.*, 1984; *Lewis and Kirwan*, 1987; *Johnson et al.*, 1992; *Vidal et al.*, 1992; *Sturges*, 1992, 1993; *Vukovich*, 1995; *Fratantoni et al.*, 1998; *Pichevin and Nof*, 1997; *Chassignet and Cushman-Roisin*, 1991]. *Hamilton* [1990] indicated that fluctuations of the Loop Current are a major source of topographical Rossby waves in the deep water. His direct current mooring measurements showed westward migration of kinetic energy in the deep water at about 9 km d^{-1} between the eastern and western gulf and suggested that fluctuations of the deep current could be interpreted as topographic Rossby waves.

[3] *Hurlburt and Thompson* [1980] numerically investigated the dynamics of the eddy shedding by the Loop Current in a idealized basin, and found that the eddy shedding rate depends on the internal Rossby wave speed and an eddy diameter derived from conservation of potential vorticity on a β plane. *Blumberg and Mellor* [1985] applied a three dimensional model to the simulation of the circulation of the Gulf of Mexico. They reproduced the seasonal cycle of the mixed layer and thermocline, but their resolution was insufficient for a realistic simulation of Loop Current shedding. By numerical experiments of a Loop Current eddy in the western Gulf of Mexico, *Smith* [1986] investigated the interaction of the eddy with topography, and suggested that the eddy motion depends on its lower layer rotational strength. The result of a modeling study implemented by *Sturges et al.* [1993] showed that dipole-like features in the deeper layer travel to the west with higher speed than the upper layer anticyclones. *Oey* [1996] examined the variability of the Loop Current and Loop Current eddies with the sigma coordinate, Princeton Ocean Model and determined optimum values of the horizontal mixing coefficient to obtain realistic results. He found a correlation between eddy shedding and decreasing or reversing lower layer (below 750 m) transports in the Yucatan Channel. *LaCasce* [1998] numerically studied quasi-geostrophic vortices on an *f* plane, and showed that the evolution of an initially symmetric vortex depends on vortex strength and size, topographic slope and ambient stratification. His results also suggested that topographically induced vertical decoupling would be quite common, as was

0148-0227/03/2001JC001074$09.00

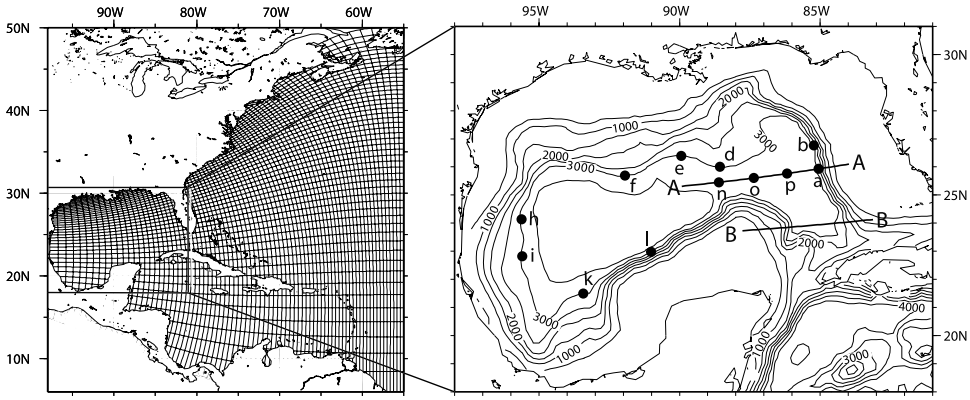

Figure 1. (left) The orthogonal curvilinear coordinate grid of the model basin. For ease of visualization every fifth contour is plotted. (right) The topography of the Gulf of Mexico with a contour interval of 500 m. Dots in the figure are the stations for the kinetic energy spectra, and the thick solid lines are the locations of the vertical sections to be discussed.

also pointed out by *Hamilton* [1990]. Anticyclonic-cyclonic pair in the deep layer beneath the Loop Current were investigated by numerical models [*Sturges et al.*, 1993; *Welsh and Inoue*, 2000].

[4] Even though results from comprehensive observational and numerical model studies have carried out, the general feature of the deep circulation and the process of the energy transition from the Loop Current of the upper layer to deep circulations have remained to be clarified. In this paper, we address two things; the process of the Loop Current and its ring shedding by using a numerical model and compare with available observations of ring frequency and path, and the lower layer circulations and its variability related to the Loop Current fluctuation. For the simulation of the deep circulations, the horizontal scale is smaller than the Loop Current in the upper layer and the topographic Rossby waves in the lower layer, we use a high-resolution ocean model. The model domain is taken west of 55°W, and this relatively large model domain minimizes the artificial boundary effect. The model is forced by realistic surface heat fluxes and wind stress fields obtained from the 3 hour Eta-29 km model, an operational atmospheric prediction model of the National Environmental Prediction Centers. This work seems to be the first numerical simulation of the Gulf of Mexico driven by realistic surface forcing.

[5] A brief description of the numerical model and model configuration is given in section 2. The shedding and translation of the Loop Current rings are investigated in section 3. Section 4 provides discussion on the deep cyclonic circulation in the eastern gulf, and the lower layer eddy induced by the anticyclonic Loop Current circulation is discussed in section 5. The average circulation and variabilities in the Gulf of Mexico are discussed in section 6, and a summary and conclusion are given in the last section.

2. Model Configuration

2.1. Numerical Model and Model Basin

[6] The numerical model used in this study is the Princeton Ocean Model [*Mellor*, 1998], which is a sigma coordinate primitive ocean circulation model with a free surface [*Blumberg and Mellor*, 1985]. The vertical diffusivity is calculated by the turbulence closure 2.5 level model of *Mellor and Yamada* [1982]. The subgrid horizontal viscosity is parameterized by the Smagorinsky viscosity [*Smagorinsky et al.*, 1965] that is a function of the gradient of the horizontal velocity (wherein the empirical coefficient is 0.05 in this study which is the value of experiment C3 in *Oey*'s [1996] study). The horizontal turbulence Prandtl number (horizontal viscosity/horizontal diffusivity) of the model is one. For the economical calculation of the free surface elevation, the vertical structure equations and the vertically integrated (external mode) equations are separately solved by a mode splitting scheme. The Boussinesq and the hydrostatic approximations are incorporated in the model.

[7] The model basin is taken west of 55°W and extends from 5°N to 50°N. There is one open boundary on the eastern border crossing the northwestern Atlantic from the Canadian Coast to the Brazilian Coast. This model domain is larger than that of previous numerical studies for the Gulf of Mexico [*Hurlburt and Thompson*, 1980; *Oey*, 1996; *Welsh and Inoue*, 2000]. The grid is constructed by a curvilinear coordinate system which has the highest resolution along the coastal region and in the Gulf Stream. The horizontal resolution in the northern shelf of the Gulf of Mexico is less than 5 km and around the Yucatan Strait the horizontal resolution is about 15 km. Figure 1 shows the entire model grid (every fifth contour is plotted) and the bottom topography in the Gulf of Mexico. The vertical resolution of the model is 25 sigma levels; the negatives of 0.0, 0.0014, 0.0028, 0.0054, 0.0106, 0.0210, 0.0418, 0.0835, 0.1668, 0.2501, 0.3334, 0.4167, 0.5000, 0.5833, 0.6666, 0.7499, 0.8332, 0.9165, 0.9582, 0.9790, 0.9894, 0.9946, 0.9972, 0.9986, and 1.0. This distribution of sigma levels is designed to resolve the dynamics of the bottom boundary layers as well as the surface boundary layers. Actual level thicknesses change with water depth. For 3500 m depth, the first and the most bottom level thickness are 4.9 m and the middle level (twelfth level) is 291.6 m.

2.2. Input Data

[8] The model is forced by realistic sea surface fluxes; wind stress, fresh water flux and net heat fluxes. Those

quantities are calculated from the 10 m atmospheric properties obtained from the 3 hour Eta 29 km data, the result of an operational atmospheric model of the National Centers for Environmental Prediction (NCEP) [*Aikman et al.*, 1996]. The Eta-29 km data is available from October 1, 1995, to May 31, 1998, and model calculations are continued by repeating the surface fluxes from June 1, 1996, to May 31, 1998.

[9] During the 6 year model run, hurricanes over the Gulf of Mexico are included in the wind forcing; 6 in 1995, 2 in 1996, 1 in 1997, and the 6 year average is 2.3/year. Based on the track data of past hurricane season by Tropical Prediction Center of National Hurricane Service, the average for 10 years (1990–1999) of hurricanes which have entered into the Gulf of Mexico is 2.5/year. The Eta-29 km data do not cover the southern region of the Caribbean Sea and the southeastern corner of the model basin. The atmospheric data over this region were extrapolated by Laplacian iteration from the border of the Eta data.

[10] Mississippi-Atchafalaya river discharge is one of the dominant factor which controls the coastal current at the inner shelf of the Texas-Louisiana Shelf [*Cochrane and Kelly*, 1986]. In the deeper region of the Gulf of Mexico, however, the effect of the river runoff is expected to be small for the Loop Current, its ring shedding process and the deep circulation during the 6 year model run. In this paper we focus on the LC and the deep circulation of the Gulf of Mexico, and the river discharge is not included in the model forcing.

[11] The model basin has open boundary along the eastern boundary at 55°W, which extends from the Canadian coast to the Brazilian coast. The vertical temperature and salinity profiles along the open boundary, 55°W, are obtained from the monthly climatological data set of the GDEM [*Teague et al.*, 1990]. The vertically integrated transport along the open boundary is estimated from the observational results of *Richardson* [1981], and the diagnostic model results of *Mellor et al.* [1982]. Comparisons of the model calculation for the Gulf Stream region will be reported elsewhere. Here the focus is on the Gulf of Mexico. The initial conditions of the model calculation are the temperature and salinity fields for October based on the GDEM data set. For the first 5 days of the model run, the temperature and density fields are fixed at the initial condition in order to spin up the velocity fields after which they are very nearly adjusted geostrophically to the initial density fields.

3. Loop Current Ring

[12] *Auer* [1987] showed that the Loop Current rings (LCRs) are generally larger than the warm-core rings of the Gulf Stream; the mean diameter of the LCRs is 222 km whereas the mean diameter of the warm-core ring of the Gulf Stream is 129 km, and LCRs less than 100 km are almost never generated in the eastern gulf. Here the formation and shedding processes of LCRs are investigated from the model results and compared with observations.

3.1. Shedding Process

[13] Figure 2 shows a time sequence of the depth fields of 20°C isotherms from months 25 to 48. A semienclosed anticyclonic circulation within the Loop Current (LC) has formed in the eastern gulf in month 25. Northward-northwestward LC penetration is developed with small morphological variations for months 26 and 27. In month 28, the LC path begins to narrow at 86°W, 25°N, and a LCR formation was not completed until after month 30. The LCR starts to move to the west and separates from the LC in month 31. The westward translation of the LCR continues until the LCR is blocked by the western boundary of the Gulf of Mexico.

[14] After shedding LCR, the LC reforms again in the eastern gulf at about 25°N in month 30 and penetrates to 27.5°N in month 33. During months 34–36, a new semienclosed anticyclonic circulation whithin the LC is fully developed, and it separates from the LC in month 40.

[15] A large undulation of the LC path is shown in month 37; the width of the LC narrows and the path elongates. In month 38, a LCR appears and separates from the LC in month 40. This pattern frequently occurs before the separation of the LCR.

[16] Comparison with the TOPEX/Poseidon altimetry data shows that the model Loop Current shedding process is quite realistic in terms of the appearance of the Loop Current intrusion and Loop Current ring shedding, the shedding period and the translation path and speed of the Loop Current rings. The sea surface height (SSH) RMS distribution of the model is in good agreement with the observational results from the satellite data. The model SSH RMS, however, is smaller than the observational results (Figure 15). The model results will be compared with the observational results more precisely.

3.2. Translation

[17] Figure 3 shows time lines of LCRs for the 72 month simulation and volume transport through the Yucatan Strait. During the simulation period there were 8 rings, labeled A through H. The average frequency of the model LCR shedding is about 270 days, which nearly equals the primary mode of eddy shedding frequency in *Vukovich*'s [1995] study, but is longer than *Auer*'s [1987] observational result of 225 days. The lifespan of rings varies from 8 months (ring B) to 4 months (ring C).

[18] *Elliott* [1982] estimated the spin down process of the LCR by the depth of 20°C isotherms from the observational results. The *e*-folding timescale of the spin down of eddies was 1.2 years, and this is longer than the life span of the model LCR (Figure 3). In order to straightforwardly compare with Elliot's observational result, *e*-folding timescale of the model LCR is estimated by the depth of 20°C isotherm. Figure 4 shows the time evolution of the maximum depth of 20°C isotherm of eight LCR's by the model. As done by *Elliott* [1982], the model results are fitted to a function, $\Delta Z = Z_o exp(-\Delta t/T_o)$, where ΔZ is the rising depth of 20°C isotherm, Z_o is initial depth of 20°C, and Δt is elapsed time. The estimated *e*-folding time from the model is 1.3 years. This is slightly longer than the Elliot's result. A question immediately arises as to why life spans of the model eddies are shorter than *e*-folding scale.

[19] Presumably the answer is related to the LCR translation length scale and speed. As shown in Figure 2, the

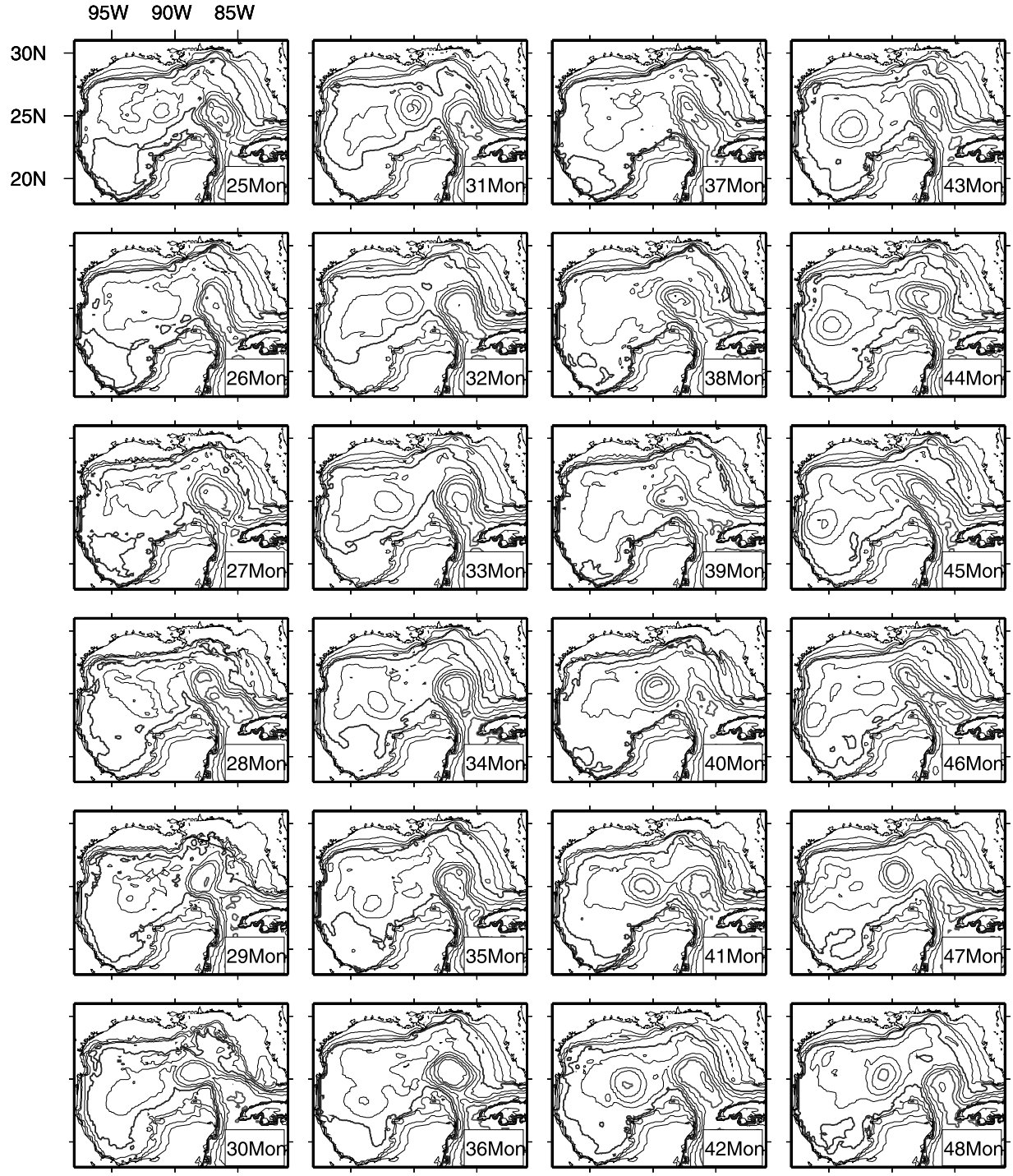

Figure 2. Snapshots of the sea surface elevations for the last day of each month from months 25 to 48. The contour interval is 0.1 m.

LCRs arrive the western boundary of the Gulf of Mexico before the *e*-folding time scale is reached. It takes 100–250 days from 90°W to 95°W with speeds of 2.14–5.32 km d^{-1}. Upon arrival at the western boundary, the strength of LCR rapidly weakens by the interaction with the slope at the western boundary of the Gulf of Mexico [*Vidal et al.*, 1999].

[20] Figure 5 shows the model tracks of the LCRs. Most model LCRs start from the region of 87°–88°W and 25°–26°N. The region where the model LCR's separate from the LC is in good agreement with the observations [*Vukovich and Crissman*, 1986]. Within the Gulf of Mexico, 88°W separates the deep basin below 3000 m into two parts, eastern and western. The junction between the eastern and western parts is where most of the model LCRs separate from the LC.

[21] The average translation angle (the clockwise angle from the north) of LCR is about 250°. This angle agrees

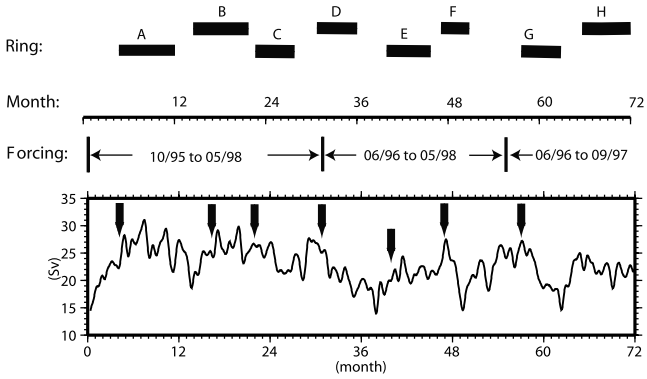

Figure 3. Life spans of the Loop Current rings from the model results. The thick solid lines represent the duration of the Loop Current rings. Periods of forcing represent the periods of the sea surface fluxes obtained from the Eta-29 km model results.

well with the average observations of 251° [*Auer*, 1987], and is smaller than the 279° observed by *Elliott* [1982]. *Vukovich and Crissman* [1986] showed three characteristic paths for the LCR (dotted lines in Figure 5), determined from the 1973–1984 satellite data. In their observational results, path 1 was the most preferred path taken by 6 rings out of a total of 8 rings. Figure 5 shows that the model LCR's paths are in agreement with the most preferred path observed by *Vukovich and Crissman* [1986].

[22] An LCR shed from the LC moves to the southwest with speeds of 2.14–5.32 km d^{-1} until it is blocked by the western boundary of Gulf of Mexico. The eddy translation speeds from the observational results obtained by *Elliott* [1982] are 2.1 km d^{-1}, 2.4 km d^{-1} by *Auer* [1987] and about 4 km d^{-1} by *Forristall et al.* [1992]. In the Gulf of Mexico, theoretical maximum phase speed of the first baroclinic Rossby wave (0.5 $\beta\lambda^2$ where λ is the

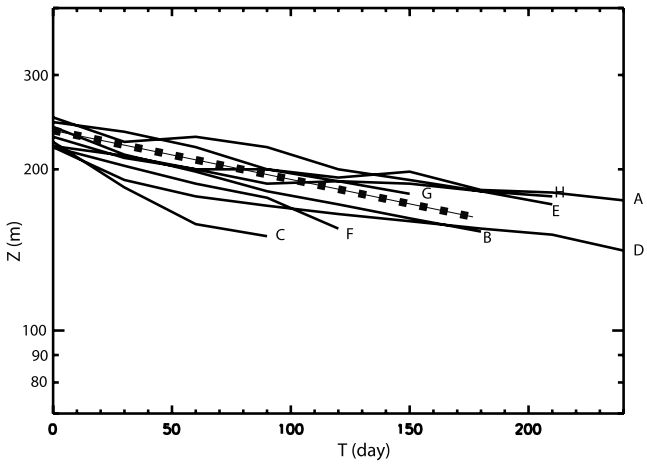

Figure 4. Temporal changes of the maximum depth of the 20°C isotherms for eight rings simulated by the model (thin solid lines) and the typical line of exponential function from model results (dotted line). ΔT represents elapsed time of each Loop Current ring from the separation.

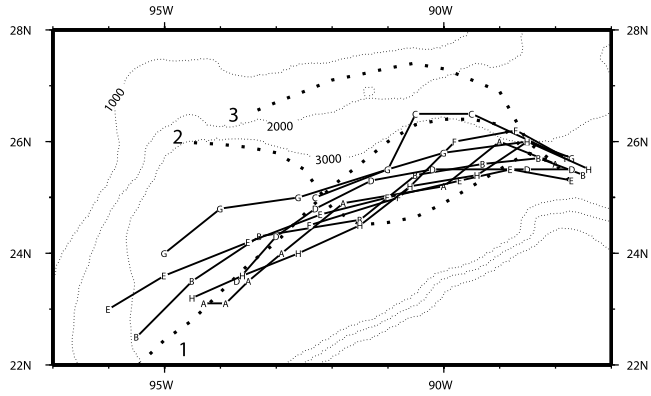

Figure 5. The trajectories of Loop Current rings from the model for the 6 year simulation. The letters on lines correspond to labels of Loop Current rings in Figure 4. Thick dotted lines are three characteristic paths for the Loop Current rings determined from the satellite data (1973–1984) by *Elliot* [1982]. The thin dotted line is the bottom topography with the contour interval of 500 m.

Rossby deformation radius) is 2.23 km d^{-1}, and most of the model LCRs and also the observations of *Forristall et al.* [1992] indicate speeds faster than the linear theoretical speed. This discrepancy also occurred in observational results. By analyzing altimetric anomalies of the satellite data, *Chelton and Schlax* [1996] found that the phase speed of sea surface height variability was generally faster than the linearized Rossby wave of the first baroclinic mode and *Zang and Wunsch* [1999] found it in the north Pacific Ocean. It has been shown that the westward phase speed of the sea surface height variability increases by the coupling of free Rossby waves with forced motions [*Qui et al.*, 1997] and by the interaction of planetary waves with zonal currents [*Kilworth et al.*, 1997].

4. Loop Current and Deep Cyclonic Circulation in the Eastern Gulf

[23] The kinematic features of the deep cyclonic circulation in the eastern Gulf of Mexico and their relation to LC movement in the upper layer are examined from the model results.

4.1. Horizontal Structure

[24] Figure 6 shows a typical sequence of the velocity fields in the eastern Gulf of Mexico at 100, 500, and 2500 m depths during the processes of LCR separation. At the depth of 100 m in month 37, the LC penetrates into the eastern gulf, and the northern boundary of the LC is near 27.5°N (Figure 6a(top)). The western limb of the LC flows to the north between the 500 and 1500 m isobaths of the continental slope, and the eastern limb is in the central portion of the eastern basin deeper than 3000 m. At the 500 m depth in month 37, the eastern limb of the LC shifts westward relative to that at 100 m. The eastern limb of the LC at 500 m depth aligned with a cyclonic circulation which occurs to the east of the LC. This cyclonic circulation, bounded by the deep eastern basin, more clearly appears at the 2500 m depth. The eastern

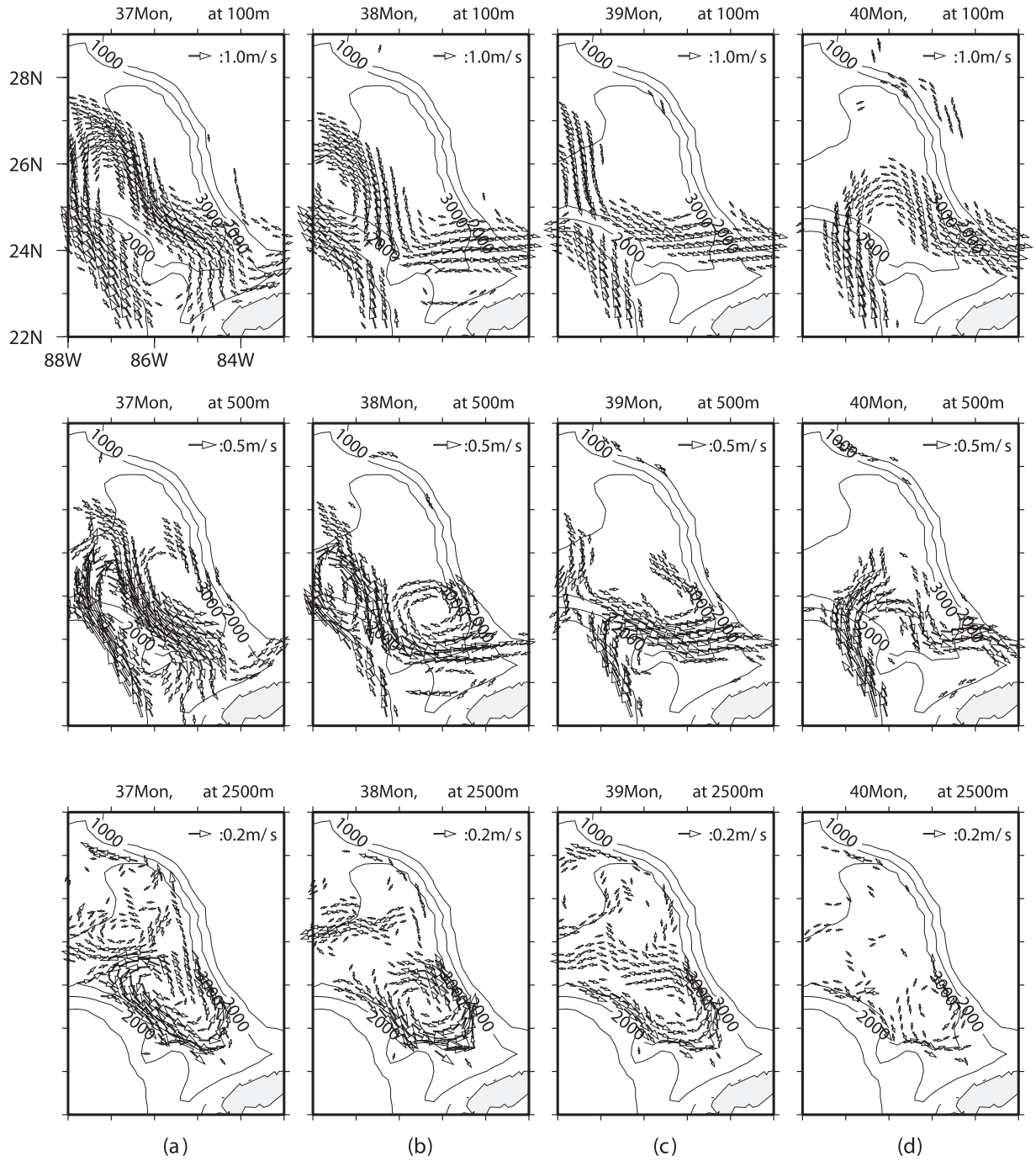

Figure 6. Horizontal velocity fields with 1 month intervals at three levels: the velocity fields (a) in month 37, (b) in month 38, (c) in month 39, and (d) in month 40 for the model results (top) at 100 m depth, (middle) at 500 m depth, and (bottom) at 2500 m depth in the eastern gulf. To emphasize the main current fields, current vectors larger than 0.3 m s^{-1} at 100 m depth, 0.15 m s^{-1} at 500 m depth, and 0.05 m s^{-1} at 2500 m depth are shown. The contour interval of depth contours is 500 m.

limb of the LC at 500 m depth is aligned with the deep cyclonic circulation.

[25] After 1 month (Figure 6b), the LC at 100 m depth is more slender due to its westward translation. An anticyclonic eddy appears at 87.5°W and 25.5°N of 500 m depth. The eastern limb of the LC feeds the cyclonic circulation east of the LC, and that feature extends to the 2500 m depth.

[26] A LCR has separated from the LC by month 39 (Figure 6c) and translates into the central Gulf of Mexico. After the LCR shedding, the LC turns back to the southern part of the eastern gulf and flows to the east at 24°N. The cyclonic circulation at 500 m depth obviously becomes weaker than that of the previous month with the cessation of the southward current at the eastern limb of the LC.

[27] The LC begins to bend to the north in month 40, and the northern limit of the LC is near 26°N. The deep cyclonic circulation almost disappears. At this stage the eastern limb of the LC is not aligned with the deep cyclone.

4.2. Vertical Structure

[28] Figure 7 shows the vertical distribution of the north-south velocity along section B in Figure 1. After passing through the Yucatan Strait the LC flows to the northern tip of the slope (87°W, 25°N). This northward western limb of the LC on the slope is restricted to the shallower region above 1500 m depth. The velocity distribution of the western limb at the Yucatan Peninsular is quit stable and keeps its path on the slope during the ring separation period (month 40) as well as during the northward intrusion period of the LC (months 37 and 43).

[29] After the separation of the LC from the slope region, the depth of the western limb (faster than 0.1 m/s) is 1200–1500 m, and the vertical distribution of the horizontal velocity maintains the velocity distribution at the Yucatan Strait (Figure 8). Below the LC, there occurs the columnar structure of the lower layer. The vertical structure of the southward eastern LC limb at the section A (Figure 8), is similar to that of the western limb. At the section B (south of the section A), the eastern limb is not symmetric with the western limb; the eastern limb is wider and especially deeper than the western limb. While the western limb is on the slope, the eastern limb extends to the bottom (3500 m) and to the eastern wall of the basin. Therefore the eastern limb of the LC at the section A vertically extends to the deep cyclonic circulation at the eastern gulf (Figures 6 and 7). This means that the upper layer LC fluctuation dominates the lower layer cyclonic circulation in the LC region through the vertical extension of the eastern limb of the LC.

[30] In month 38, the eastern limb of the LC moves to the west, and the cyclonic circulation occurs almost barotropically in the eastern basin (Figures 6 and 7). It is noticed that there is the maximum northward velocity (solid line in month 38, Figure 7), 0.2 m s^{-1}, of the deep cyclonic circulation near the bottom, indicating the bottom intensification. After 1 month, the LCR has separated from the LC. The eastern limb of the LC almost disappears in the upper layer, and the southward current of the deep circulation weakens. In month 40, the deep circulation ceases, and a new eastern limb appears at the eastern region. The transient feature is shown in month 41; the distance between eastern and western limb is 250 km due to the northward penetration and the westward movement of the LC, and the deep cyclonic circulation is not developed in the eastern gulf. When a new semienclosed anticyclonic circulation is fully developed in month 42, the eastern limb of the LC reappears and the deep cyclonic circulation strengthens again.

[31] The deep cyclonic circulation is kinematically linked to the LC; the southward eastern limb of the LC continued to the deeper layer and feeds the cyclonic deep circulation. The deep cyclonic circulation is developing when the southward limb of the LC is at the central region of the eastern gulf (month 37 and month 42 in Figure 7). Thus the state of the deep circulation can be inferred from the position of the LC eastern limb.

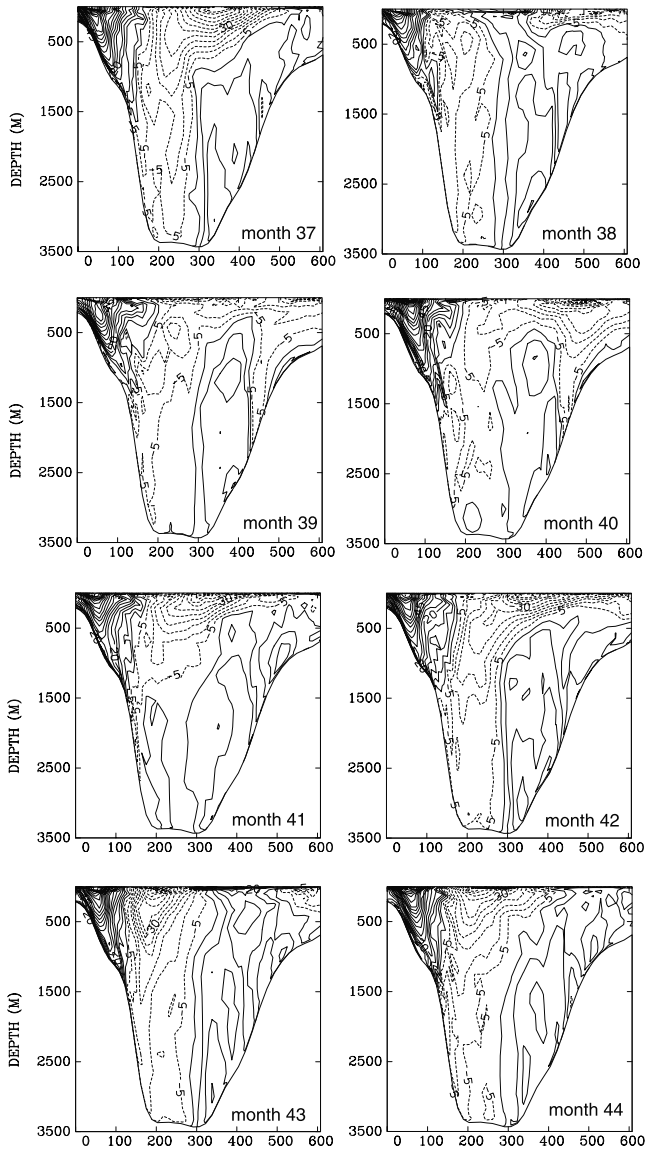

Figure 7. Vertical section of the north-south velocity along section B in Figure 1 from months 37 to 44. Solid lines are northward velocities, and dashed lines are southward velocities. The contour interval is 5 cm s^{-1}.

5. Loop Current and Lower Layer Eddy

[32] The horizontal scale of the Loop Current is generally two or four times the Rossby radius of deformation for the first baroclinic mode (Figure 2). A surface vortex with this size and slope can induce dispersive topographic waves in the lower layer [*LaCasce*, 1998]. *Hurlburt and Thompson* [1980] showed that wave energy is transferred from upper to lower layer in a rectangular flat bottomed basin, due to the baroclinic instability. *Oey* [1996] also mentioned the upper to lower transfer of the energy through baroclinic instability in a Loop Current ring. Here, it will be shown that LC penetration induces lower layer

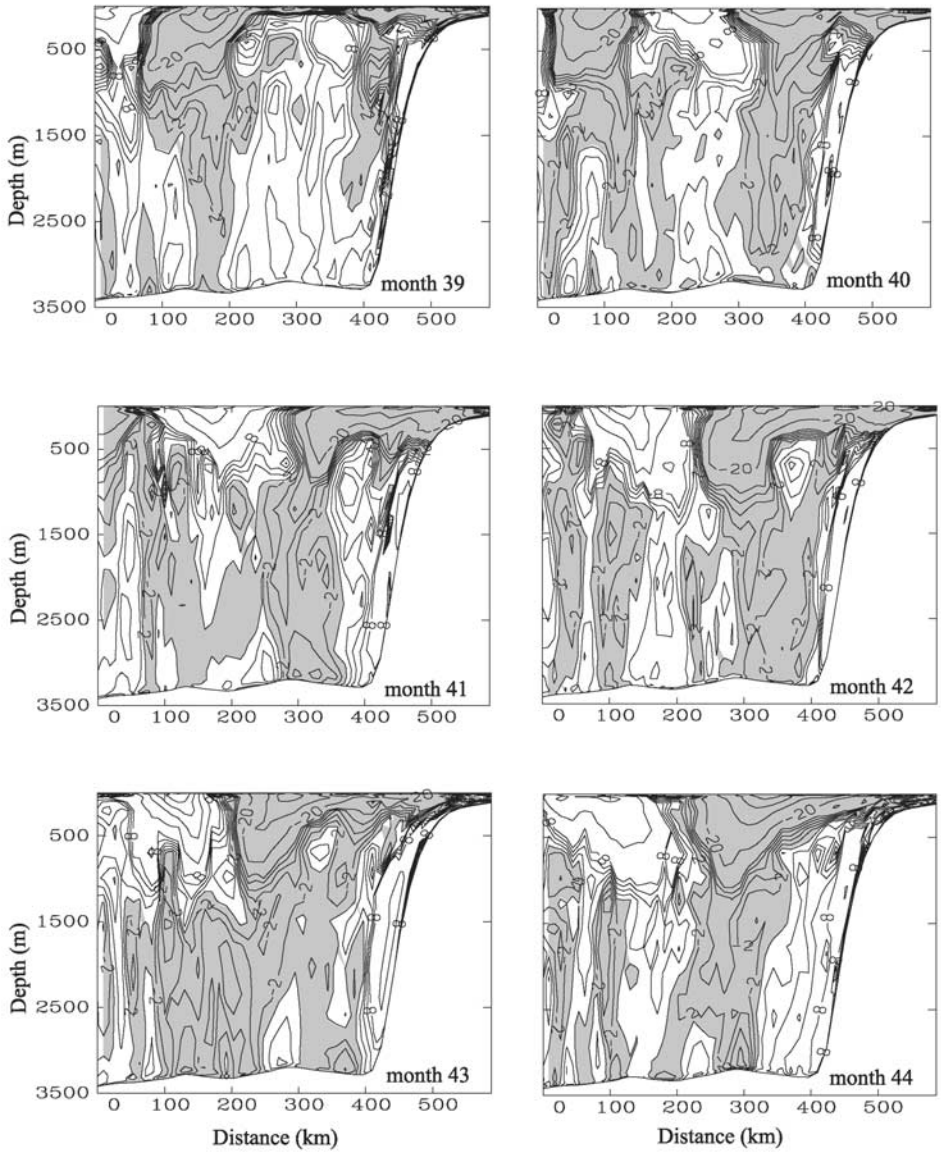

Figure 8. Vertical section of the north-south velocity along section A in the Figure 1 from months 39 to 44. The shaded area denotes southward velocity. The contour (solid line) interval is 10 cm s^{-1}. Dashed contours represent velocity slower than 10 cm s^{-1} with the contour interval of 2 cm s^{-1}.

eddies in the eastern gulf followed by detachment of the lower eddies from the LC.

5.1. Lower Layer Eddies

[33] Figure 8 is the snapshot of the north-south velocity section on the last day of each month along transect A of Figure 1. The vertical structure of the model LC is limited to the upper 1500 m depth which agrees with observations [*Elliott*, 1982; *Forristall et al.*, 1992]. In Figure 8, the lower layer columnar eddies under the LC, and the detachment of the lower layer eddies from the LC are clearly shown. In month 42, the columnar eddy structure deeper than 1000 m depth occurs under the LC, and similar patterns appear in months 39, 40, and 44.

[34] A northward current occurs along the slope of western Florida below 500 m. This current is the eastern limb of the deep cyclonic circulation described in previous section; a current maximum appears about at 2000 m depth. The lower layer columnar eddy under the LC disappears in months 41 and 43; these eddies are detached from the upper layer and move to the west.

5.2. Detachment of the Lower Layer Eddy From the Loop Current

[35] The detachment process of the lower layer eddies from the LC is seen in Figure 9, which shows the time variation of the north-south velocity along transect A (Figure 1). The time variation at the 300 m depth mainly represents the LC and the LCR. From months 33 to 37, the LC generally maintains its position; after month 37, a model LCR detaches. The LCR then translates to the west with the velocity of 3.20 km d^{-1}. During the developing period (months 33–37), the lower layer eddies detach from the LC and move to the west; the eddy translation

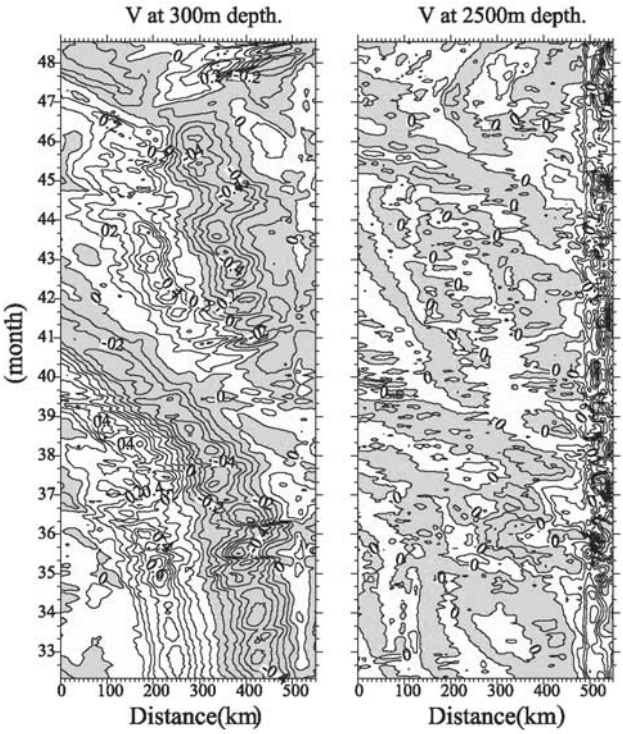

Figure 9. Time-distance diagram of the north-south velocity along section A (Figure 1) at (left) 500 m depth and (right) 2500 m depth from days 980 to 1460. Southward velocity is shaded. The contour interval is 0.1 m s^{-1} in the Figure 9 (left) and 0.05 m s^{-1} in the Figure 9 (right).

begins in months 33–35 (Figure 9 (left)). In month 37, at the beginning of an LCR shedding, a lower layer eddy also moves to the west. As the LCR sheds, the lower layer eddies, through fragmented, move to the west with velocities of 6.05–6.91 km d^{-1} which is almost twice as fast as that of the LCR. Figure 8 of month 38 shows the model result after the LCR shedding. It is seen in this snapshot that the lower layer columnar eddy is tilted to the west with depth, due to the difference of translation speeds between upper and lower layer.

[36] As shown in Figure 9, the translation speed of the lower layer eddy (6.0–7.0 km d^{-1}) is twice as fast as that of the upper layer (3.0–3.5 km d^{-1}). In the upper layer, the Rossby wave with the planetary beta dominates the westward translation. In the quasi-geostrophic dynamics of the lower layer, the topographic beta prevails over the planetary beta, and the westward translation of the columnar eddy can be explained by the Topographic Rossby waves [*Oey and Lee*, 2002]. This difference of beta effects in the quasi-geostrophic dynamics induces the separation of the lower layer eddies from the upper layer rings by different translation speeds.

[37] It is noted in Figure 9 that the fast westward translation (6.0–7.0 km d^{-1}) of the lower layer eddies takes place in the western part of the section A (to the west of about 300 km), and this is due to the difference of bottom slope. The topography of the eastern part of the section A is almost flat, and the topographic gradient and the topographic beta effect are also very small. The topographic gradient of the eastern region is less than 1×10^{-3}, and the gradient of the western region is about 5×10^{-3}. Therefore, the Topographic Rossby wave is supported only in the western region of the section A. In the lower layer (below 27.5 σ_t) of this western part, the Brunt-Vaisala frequency calculated from the temperature and salinity profiles of the Levitus climatological data is about 1×10^{-3} s^{-1}. The horizontal scale of the lower layer eddy is about 110 km (Figures 8 and 9). Then, the westward phase speed of the Topographic Rossby wave calculated from those conditions is 7.6 km d^{-1}, and this is in agreement with the translation speed of the model lower layer eddy (6.0–7.0 km d^{-1}).

5.3. Dynamic Modes and EOF Modes

[38] To investigate the vertical structure and variability of the velocity profiles, three points (stations n, o, and p) on section A (Figure 1) are selected. Figure 10 shows strongly baroclinic velocity profiles in the upper layer and nearly barotropic lower layer eddies below 1500 m. At station p the southward flow of the lower layer is closely correlated with a fast southward LC upper layer. There are short period north-southward velocity fluctuations or the northward velocity fluctuations at the lower layer when the upper layer Loop Current is weak. However, at station n the lower layer velocities are uncorrelated with the upper layer motions due to the westward translation of the lower layer eddies which were formed farther to the east.

[39] It is of interest to examine the dynamic modes for these stations. The density profiles of the three stations were nearly identical. The average Brunt-Väisälä frequency, $N(z)$, for the 6 year model run are shown in Figure 11a. Strong stratification exists in the upper 1000 m and weak stratification in the lower layer.

[40] Solutions to the quasi-geostrophic Rossby wave equation,

$$\frac{\partial}{\partial t}\left[\nabla_h^2\psi + \frac{\partial}{\partial z}\left(\frac{f^2}{N^2}\frac{\partial \psi}{\partial z}\right)\right] + \beta\frac{\partial \psi}{\partial x} = 0 \tag{1}$$

and boundary conditions, $\partial\psi/\partial z = 0$ at $z = 0$ and $z = -H$, are

$$\psi = \phi(z)e^{kx+ly-\sigma t} \tag{2}$$

where the horizontal velocities, (u,v) = $(\partial\psi/\partial y, -\partial\psi/\partial x)$ and where the frequency and westward propagating phase velocities are

$$\sigma_n = \frac{-k\beta}{k^2 + l^2 + \mu_n^2} \tag{3}$$

$$(c_x, c_y) = -(1, k/l)\frac{\beta}{k^2 + l^2 + \mu_n^2} \tag{4}$$

The eigenfunctions, $\phi(z)$, and eignevalues, μ_n, corresponding to the average $N(z)$ are shown in Figure 11a together with the nondispersive phase velocities, $-(1,k/l) \cdot \beta/\mu_n^2$, and group velocities, $(c_{gx}, c_{gy}) = (c_x, 0)$.

[41] The zero crossing of the first baroclinic mode is at about 700 m depth, and profiles of first three modes are almost vertically constant below 1500 m. The phase speed of nondispersive Rossby waves of the first baroclinic mode is 2.16 km d^{-1}. The average westward translation speed of

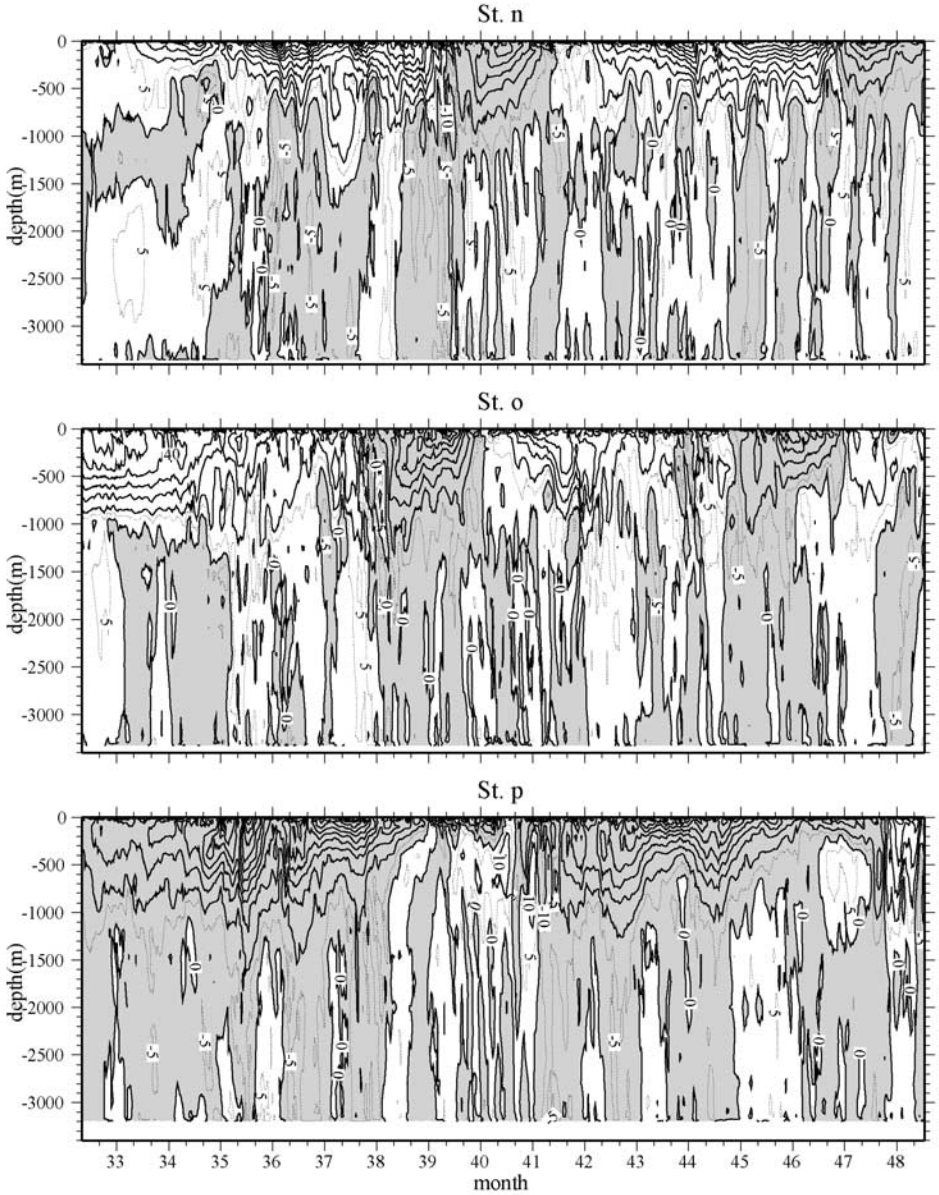

Figure 10. Time-depth diagram of north-south velocity at stations n, o, and p (Figure 1). Southward velocity is shaded. The contour interval of solid lines is 0.1 m s^{-1}, and the contour interval of dotted lines is 0.05 m s^{-1} between -0.1 and 0.1 m s^{-1}.

the model Loop Current rings at section A is about 3.2 km d^{-1} (Figure 9). Thus, the model result is faster than the speeds of linearized theory. A similar discrepancy between observed Rossby wave speed and linear theory has been noted and researched by *Chelton and Schlax* [1996] and *Zang and Wunsch* [1999].

[42] There are other singular solutions corresponding to $-m^2 \equiv \mu^2 \leq 0$ and the bottom boundary conditions,

$$\frac{\partial^2 \psi}{\partial t \partial z} = \frac{N^2(-H)}{f}\left(\frac{\partial \psi}{\partial y}H_x - \frac{\partial \psi}{\partial x}H_y\right), \tag{5}$$

$$\frac{\partial \phi}{\partial z} = -\frac{N^2(-H)}{f\sigma}\left(lH_x - kH_y\right). \tag{6}$$

and where $(H_x, H_y) \equiv (\partial H/\partial x, \partial H/\partial y)$.

[43] We have numerically solved the problem for the same $N(z)$ as shown in Figure 11b and for multiple values of mH. Remarkably, we find, to very good approximation, that $m = 6.67\ (lH_x - kH_y)\ f\sigma^{-1}$. Now, it may be shown that, generally, m^2 and $k^2 + l^2 \gg k\beta/\sigma$ so that, from equation (3), we have $m^2 = k^2 + l^2$ and

$$\sigma = -6.67 f \frac{kH_y - lH_x}{(k^2 + l^2)^{1/2}} \tag{7}$$

Note that the constant, 6.67, is related to the specific in situ $N(z)/f$ where $N(z)$ is given in Figure 11a.

[44] To simplify the equations, we can align our coordinate system such that $H_x = 0$. Then the phase and group velocities may be written

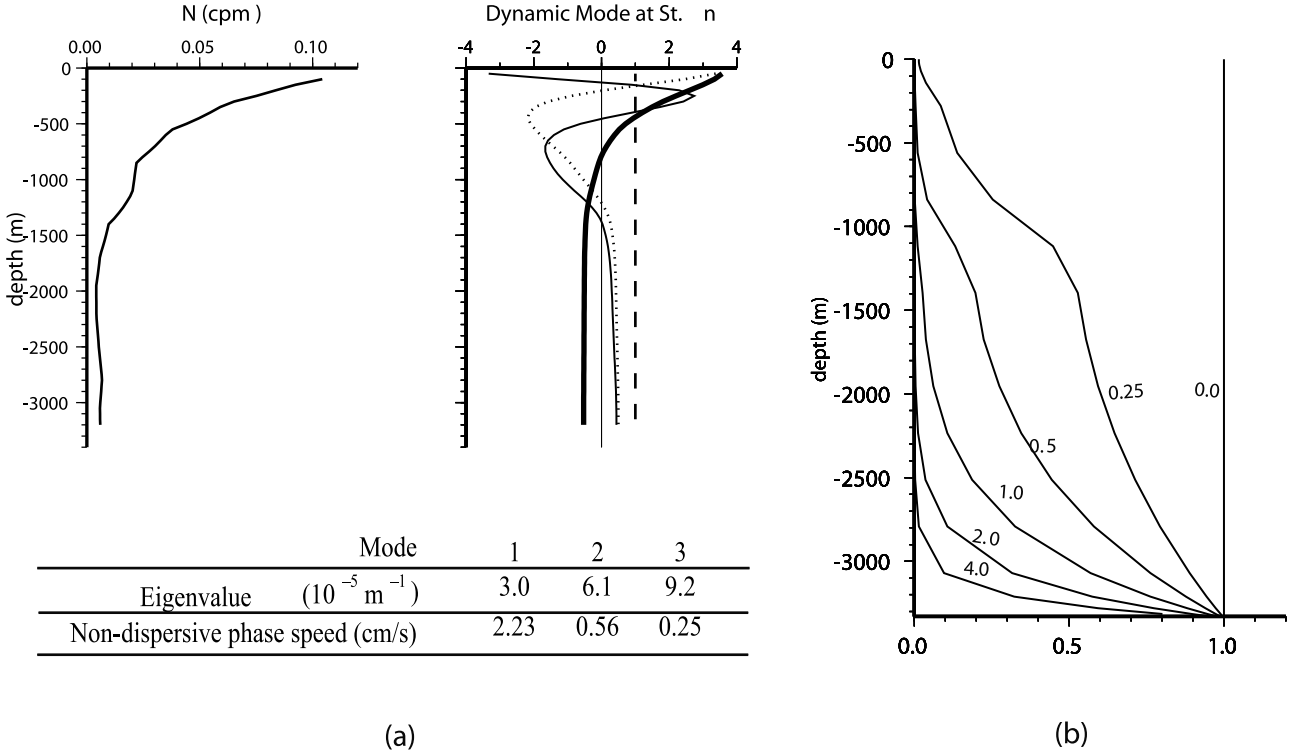

Mode	1	2	3
Eigenvalue (10^{-5} m^{-1})	3.0	6.1	9.2
Non-dispersive phase speed (cm/s)	2.23	0.56	0.25

Figure 11. (a) Vertical profiles of averaged Brunt-Väisälä frequencies for the 6 year model run and dynamical modes: barotropic mode (thick dashed), the first (thick solid), the second (dotted), and the third baroclinic mode (thin solid). (b) Vertical profiles of a singular solutions corresponding to $-m^2 \equiv \mu^2 \leq 0$ and the bottom boundary conditions associated with slope (see text). The labels are values of mH.

$$(c_x, c_y) = -\frac{6.67 f H_y}{(k^2+l^2)^{1/2}}\left(1, \frac{k}{l}\right) \tag{8}$$

$$(c_{gx}, c_{gy}) = -\frac{6.67 f H_y}{(k^2+l^2)^{3/2}}(l^2, -kl) \tag{9}$$

Therefore, in the case of $H_y > 0$, the phase propagates westward and downslope, and the wave energy moves to the westward and upslope when $kl > 0$.

[45] The profiles for different values of mH are shown in Figure 11b; when $m > 0$, velocities are intensified near the bottom. The bottom intensification is shown in Figure 8, snap shots of vertical section of horizontal velocity. In every month, the maximum velocity below 2000 m depth occurs at the bottom; the maximum bottom velocity is more than 8 cm s^{-1}.

[46] An EOF decomposition is applied to the velocity data of Figure 10. One sees that at station O and P, the first EOF mode appears to be a superposition of the first baroclinic mode and the barotropic mode. the EOF modes (Figure 12) have similar patterns to the first three dynamic modes. If the correspondence were exact, the dynamic modes would be uncorrelated in time [*Kundu et al.*, 1975]. However, to more closely approximate the EOFs, a linear combination of dynamic modes is required.

[47] The first EOF mode explains more than 80% of total variance (Figure 11). The amplitude of the first EOF mode increases rapidly near the surface and is very small below 1500 m depth. Kinetic energy spectrums of amplitudes of first three EOF modes at stations n, o, and p are shown in Figure 13. The maximum peak of the first mode at St.p is at the eddy shedding period of about 290 days. Dominant fluctuations in three stations are 0.01–0.03 cpd.

[48] Large undulations of the LC path are shown in months 37 and 38 (Figure 2), and the LC crosses over stations n and o before the separation of the LCR. Thus the peaks of 1st EOF at stations n and o have shorter period than one at station p.

6. Averaged Flow Pattern and the Variability

6.1. Averaged Circulation in the Gulf of Mexico

[49] *Blaha and Sturges* [1981] have suggested that a basin wide anticyclonic circulation and a Gulf Stream-like western boundary current could be driven by wind stress curl at the surface. *Sturges* [1993] showed that a local wind stress curl does drive annual variations of the western boundary current. From hydrographic data, *Vidal et al.* [1999] showed that a western boundary current was set up by the interaction of LCR with the slope of the western gulf, and this is the main forcing mechanism in the regional circulation. Figure 14 shows 6 year average current fields at the surface (Figure 14a) and at the 2000 m depth (Figure 14b) from the model results. The principal feature of the surface circulation is the anticyclonic circulation over the gulf, which is consistent with ship drift data [*Sturges*, 1993]. A relatively strong anticyclonic circulation appears in the eastern gulf related to the Loop Current and an eastward current flows along the Louisiana continental shelf break (it is noted that the river runoff is not included in this model).

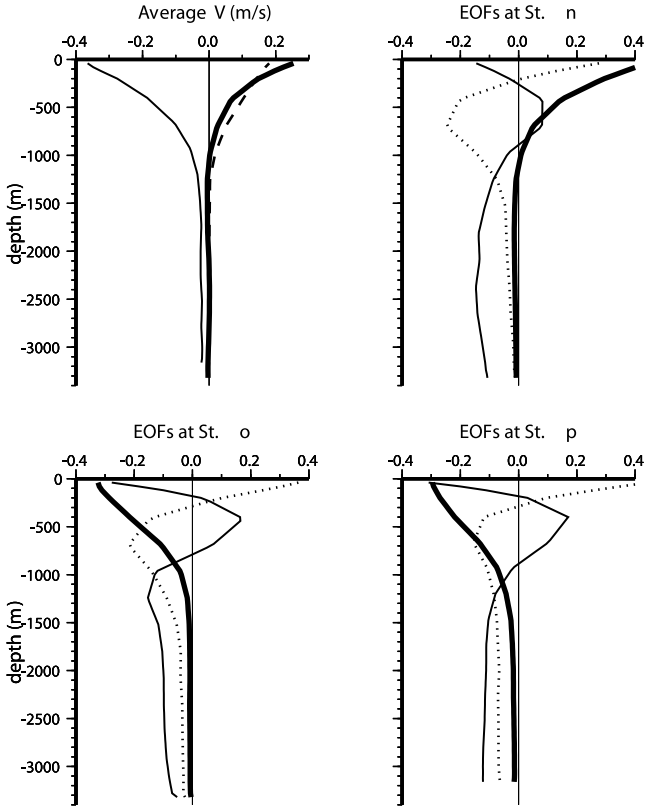

Figure 12. Vertical profiles of averaged north-south velocities for the 6 year model run, and the first three EOF modes. Thick solid, dotted, and thin solid lines denote the first, second, and third EOF modes, respectively.

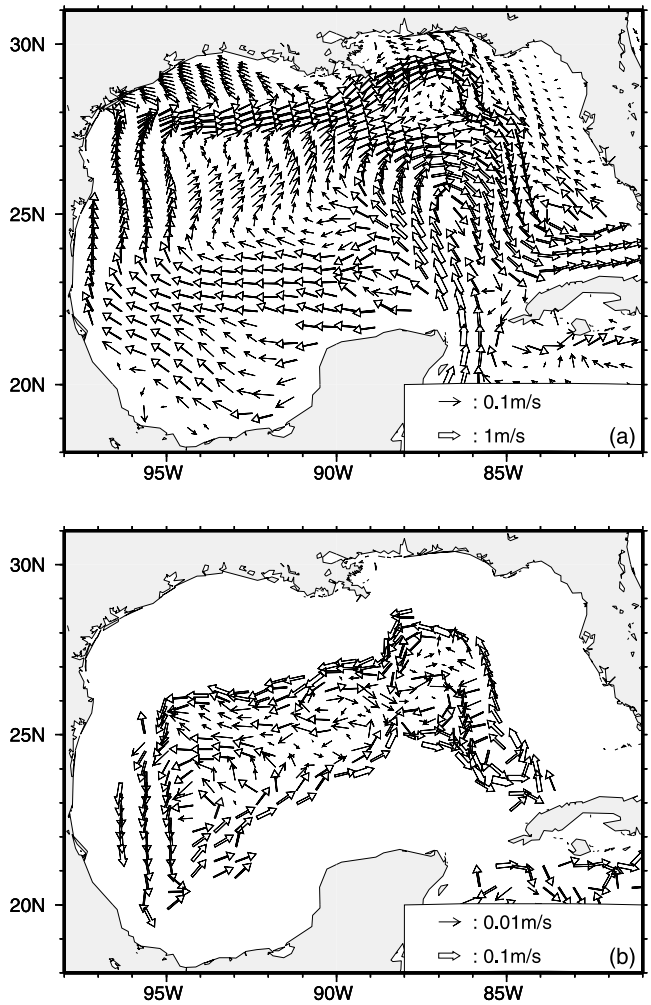

Figure 14. Six year averaged velocity fields at (a) the surface and (b) 1500 m. The width of arrows represent the speed of flow.

[50] In the model results the western boundary current is weak and wide; the width of the current in the model is 200–300 km, which is about one order larger than the Munk layer. In synoptic sea surface elevations of Figure 2, the anticyclonic circulation occurs in basin scale, but the western boundary structure akin to the Gulf Stream or the Kuroshio is not evident.

[51] As suggested by *Blaha and Sturges* [1981] and *Sturges* [1993], the wind stress fields of the Gulf of Mexico drives the basin wide anticyclonic circulation and seasonal variation of the western boundary current. In addition to this, model results show that the anticyclonic circulation of the Gulf of Mexico largely affected by the average effect of LCRs, which have migrated to the west dispersing anticyclonic vorticity.

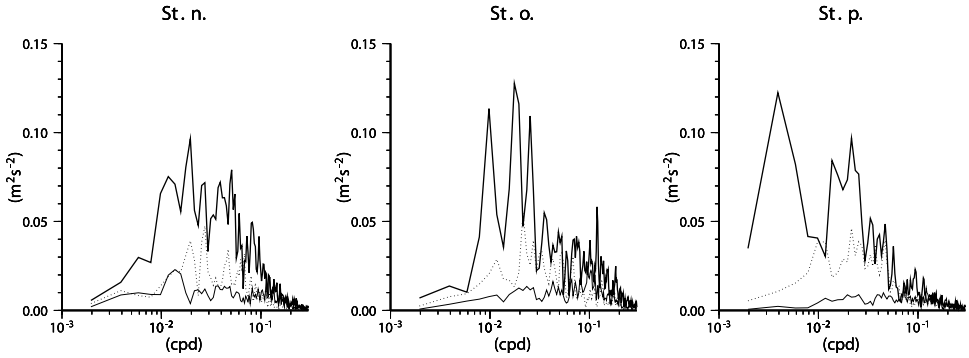

Figure 13. Kinetic energy spectra for amplitudes of the first three EOF modes at stations n, o, and p. The spectra is in variance-preserving form and has 8.4 degrees of freedom, and the bandwidth is 0.00195 cpd. Thick solid, dotted, and thin solid lines denote the first, second, and third EOF modes, respectively. It is noted that the LCR shedding frequency is about 0.0035 cpd.

[52] In the deeper layer, a cyclonic circulation that is the reverse of the upper layer circulation occurs along the continental slope and is guided by the bottom topography. The westward current at the Louisiana slope converges and diverges following the steepness of topography (Figure 1). A deep cyclonic circulation is in the southeast corner of the gulf, which is surrounded by steep slope.

[53] Depths of the Florida Strait and the Yucatan Channel are shallower than 2000 m, and the deep circulation of the Gulf of Mexico below 2000 m depth is isolated from the deep circulation of adjacent seas. Thus, it is expected that the deep circulation of the gulf is caused by the upper layer. As was shown previously, the deep cyclonic circulation in the eastern gulf is driven by the LC fluctuation of the upper layer, especially by the eastern limb of the Loop Current. The model result (Figures 7 and 8) shows that the eastern limb of the Loop Current which flows to the south barotropically extends to the bottom, and this barotropic extension of the southward flow induces the cyclonic circulation at the lower layer along the U-shaped deep basin in the western gulf. This suggests that the deep cyclonic circulation of the eastern gulf induced by the upper layer Loop Current is important in terms of the energy source of the deep circulation in the Gulf of Mexico.

6.2. Variability of Sea Surface Height

[54] Figure 15 shows the 6 year average sea surface height (SSH) of the model, the RMS SSH distribution of the model, and the RMS SSH of the TOPEX/Poseidon (T/P) data from October 1992 to June 1996. The averaged Loop Current path is shown in the eastern gulf (Figure 15a) as a smoothed pattern. A SSH ridge appears in the deep and central region west of 89°W. The orientation of the SSH ridge is about 250°, which agrees with the direction of the LCR translation of the model and observations [*Elliott*, 1982; *Auer*, 1987]. This implies that the SSH distribution in the middle and west gulf is largely influenced by the LCR propagation.

[55] The large variability of the model and the observational SSH occurs in the eastern gulf due to the Loop Current fluctuations. The location of the maximum peaks from the model results agrees with the T/P result, but the maximum value of the model is smaller than the observations; 0.2 m in the model and 0.3 m in the T/P observations. This discrepancy of the maximum RMS is partly due to the less LC transport of the model (22.7 Sv) than observations (25.8–27.1 Sv). Under the simple linear assumption that the change of the LC transport geostrophically affects only the amplitude of sea surface height fluctuations (not the LC path and variability), the less transport of the model LC can explain 40% of the maximum RMS discrepancy. The remaining 60% of the RMS discrepancy may result from the less variability of the model LC related to the nonlinear undulation and small scale frontal structures. The horizontal viscosity also affects the RMS SSH distribution of the model. As shown by *Hurlburt and Thompson* [1980], the strong undulation of the Loop Current took place when a model horizontal viscosity is reduced. Thus it is expected that the RMS generally increase with decreasing horizontal viscosity.

6.3. Kinetic Energy Spectra

[56] The kinetic energy (KE) spectra at 600, 1500, and 2400 m depth following the 3000 m isobath (Figure 1) are shown at Figure 16, station a in the eastern gulf, which is near the mooring position of A and G by *Hamilton* [1990]. The spectral peak at the 600 m current is 0.015 cpd, and peaks at 1500 and 2400 m are 0.03–0.05 cpd. At station b the predominant peaks of spectra occur about 0.025–0.04 cpd. These peaks are identified in the numerical simulation of the Gulf of Mexico by *Oey* [1996]; the intensification with depth occurs at frequency 0.01 and 0.02–0.03 cpd in the eastern gulf. The variance of the spectra at stations a, b, and p are less than Hamilton's observational results, but the spectral patterns agrees with his observations [see *Hamilton*, 1990, Figure 4]. The current at 1500 m at station b is more energetic than the upper or lower layer currents. Station d is at the outlet of the eastern gulf, and the spectral peaks occur at 0.02 and 0.03 cpd. The deep current at 2400 m depth is

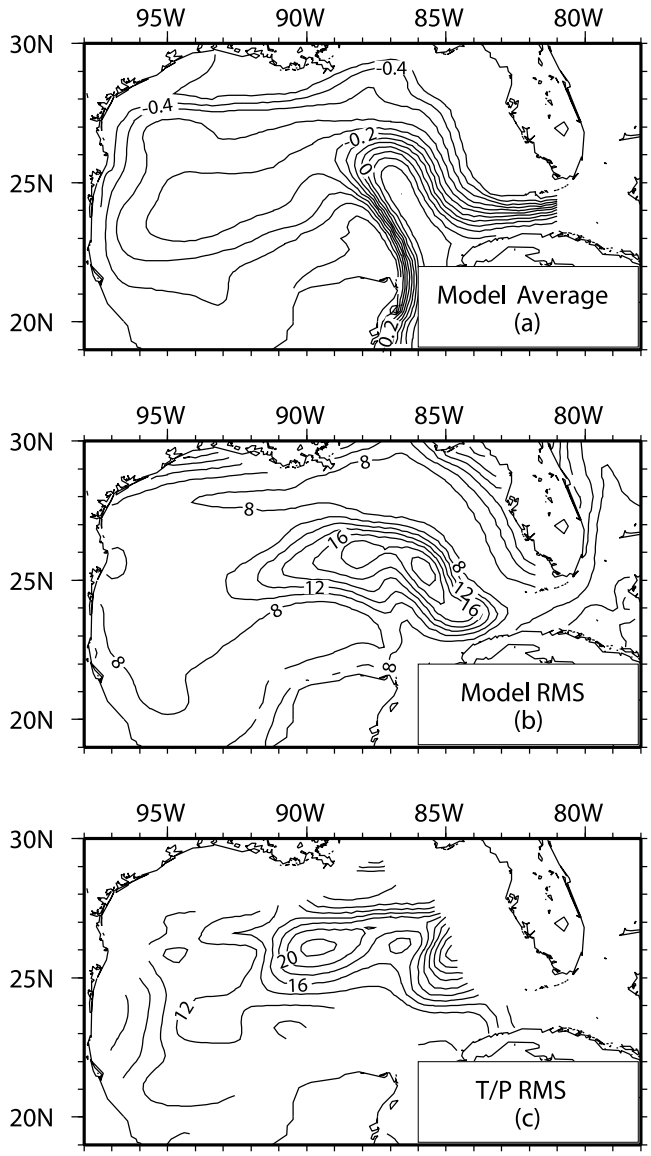

Figure 15. The horizontal distribution of (a) the 6 year averaged sea surface elevation, (b) the RMS of the sea surface elevation, and (c) the RMS of TOPEX altimetry data from October 1992 to June 1996. The contour intervals are 0.05 m in Figure 15a and 2 cm in Figures 15b and 15c.

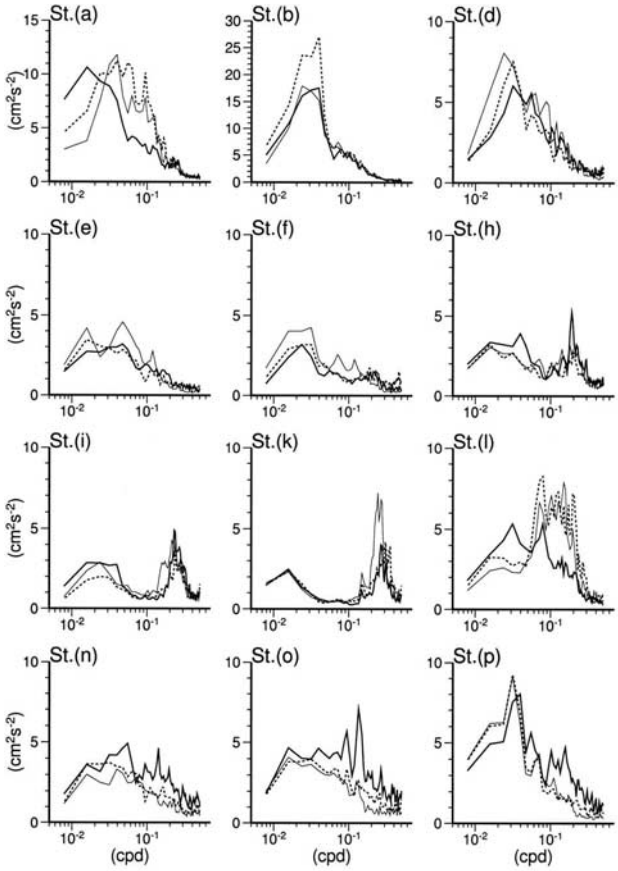

Figure 16. The kinetic energy spectra at the stations in Figure 1 at 600 m depth (thick solid line), 1500 m depth (dashed line), and 2400 m depth (thin solid line). The spectra are in variance-preserving form and have 33.6 degrees of freedom, and the bandwidth is 0.00781 cpd.

more energetic than intermediate and upper layer current. This bottom intensification occurs at the central gulf region of stations e and f.

[57] At stations h and i in the western gulf, the lower-frequency band of 0.015–0.04 cpd is similar to those of stations e and f in the central gulf, and these spectral peaks are also shown in the *Oey* [1996] results in the western gulf. There is a high-frequency fluctuation of about 0.2–0.25 cpd in the western gulf.

[58] *Brooks* [1984] carried out mooring observations in the western gulf and showed that the Loop Current rings play an important roles in current and hydrographic variability in the western gulf. In his observational result at 450 m depth (dashed line in Figure 6 of *Brooks* [1984]), there were energy peaks in 0.2–0.3 cpd, and that is in agreement with the model result at 600 m depth in the western gulf (stations h, k, and i). Thus it seems that this high-frequency model fluctuation of 0.2–0.3 cpd in the western gulf is due to the interaction of the Loop Current rings and the continental slope.

6.4. Low-Frequency Fluctuations in the Eastern Gulf

[59] Figure 17 compares the low-frequency (100 day low-pass filtered) variations of the volume average kinetic energy and relative vorticity in the upper layer (upper 27.5 σ_t isopicnal) and the lower layer (lower 27.5 σ_t isopicnal) of the eastern gulf (east of 89°W and region deeper than 3300 m depth). The most energetic fluctuation of the LC is the LCR shedding process with about 10 month period. The kinetic energy (KE) of the lower layer is one order smaller than the upper layer (the average KEs are 0.077 and 0.007 $m^2\ s^{-2}$ at upper and lower layer), however, the variation of the lower layer is similar to that of the upper layer (Figure 17). The minimum of KE in the lower layer occurs when the LCR is shedding, and the maximum occurs when the LC is fully developing. This assures that the deep circulation in the eastern gulf closely links with the LC fluctuation; the lower layer circulation strengthens by the eastern limb of the LC when the LC is developing and intrudes to the north (Figure 6a), and the deep circulation weakens when the LC locates south of 25°N (Figure 6c) after the LCR shedding. The correlation of the low-frequency KE fluctuation between upper and lower layer is 0.71. The RMS of KE of upper layer is 0.0524 $m^2\ s^{-2}$ and that of lower layer is 0.0058 $m^2\ s^{-2}$, which is 10.7% of the upper layer RMS.

[60] The variation of the upper layer depth (Figure 17c) defines the fluctuation of the LC. The upper layer depth increases when the LC intrudes to the north, and decreases after the LCR shedding. The variation of the lower layer depth is opposite to that of the upper layer because the height of whole water column is to be conserved; the amplitude of the sea surface height is almost two orders of magnitude less than that of 27.5 σ_t isopycnals.

[61] It is noted that the lower layer relative vorticity (normalized by the Coriolis parameter) is always cyclonic. In terms of the potential vorticity constraint, the variation of the relative vorticity in the lower layer is consistent with the variation of the lower layer depth. When the lower layer depth is increasing (stretching), the relative vorticity is also increasing (cyclonic).

[62] The model results show that the northward intrusion of the LC, developing of the cyclonic circulation in the lower layer and the lower layer shrinking take place at the same time. The correlation between the lower layer vorticity and the lower layer KE is 0.85, and this is larger than the correlation between the lower layer relative vorticity and the lower layer depth (0.66). This supports that the mechanism maintaining the cyclonic vorticity in the lower layer is the upper layer LC fluctuation; when the LC intrude to the north, the cyclonic circulation is developing in the lower layer by the eastern limb of the LC (Figure 6), and because of the warm water intrusion in the upper layer the lower layer is shrinking.

7. Summary and Conclusion

[63] Using the Princeton Ocean Model, a numerical study is performed for the northwest Atlantic Ocean and the Gulf of Mexico. Here we focus on the latter basin, and the dynamics of the Loop Current, Loop Current rings and concomitant deep circulation.

[64] Undulations of model LC paths occur before the separation of the LCR. For the six year simulation, eight rings separated from the LC. These LCRs move to the southwest with the average translation angle of 250° and

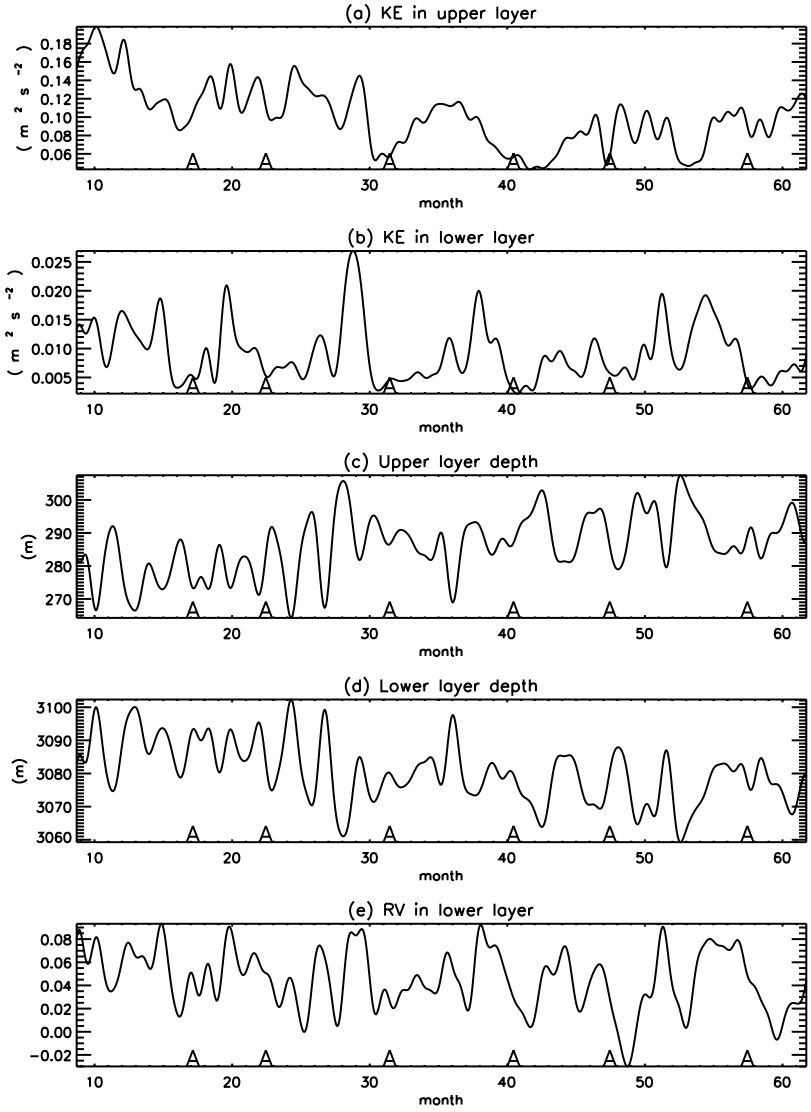

Figure 17. (a) Time series of the average kinetic energy in the eastern Gulf of Mexico in the upper layer (surface to 1000 m depth); (b) the average kinetic energy in the lower layer (1000 m depth to bottom); (c) the averaged relative vorticity of the upper layer normalized by the Coriolis parameter; and (d) the same as Figure 17c but in the lower layer. Those quantities are obtained over the area deeper than 3300 m depth of the eastern gulf (east of 89°W). "A" in the figure indicates the Loop Current ring shedding.

speeds of 2.14–5.32 km d^{-1} in accord with observational results [*Elliott*, 1982; *Auer*, 1987; *Forristall et al.*, 1992; *Vukovich*, 1995]. The nondispersive Rossby wave of the first baroclinic mode is about 2.2 km d^{-1}. As the LC penetrates into the Gulf of Mexico, the western limb of the LC flows to the north between the 500 m and 1500 m isobaths of the continental slope, and the eastern limb is in the central region of the eastern basin deeper than 3000 m. Model results show that these deep cyclonic circulations are developed by the LC fluctuation in the upper layer. While the northward intrusion of the LC is occuring, the eastern limb of the LC generates the deep cyclonic circulation which is nearly barotropic below 500 m depth and bounded by the basin slope of the eastern Gulf of Mexico. After the Loop Current ring shedding, the LC turns to an eastward flow around 24°N and begins to penetrate into the north. At that time, the flow direction of the LC is opposite to the deep cyclonic circulation, and the deep cyclone is spinning down.

[65] The semienclosed anticyclonic circulation of the LC penetration induces anticyclonic lower layer eddies in the eastern Gulf of Mexico in the model. The lower layer eddy occurs deeper than 1000 m depth under the LC and has a columnar structure. These lower layer eddies are detached from the upper layer LC and move to the west with speed of 6.1–6.9 km d^{-1}. The westward translation speed of the LCR is about 2.16–5.18 km d^{-1}, and therefore the lower layer eddies enter the central gulf first.

[66] The nodal point of the first baroclinic mode is about 700 m, and profiles of first three dynamic modes are nearly homogeneous below 1500 m. The phase speed of nondispersive Rossby waves of first baroclinic mode is 2.16 km d^{-1} in the eastern gulf, whereas the nonlinear ring translation speed is 3.7 s^{-1}. The EOF modes for the velocity in

the eastern gulf resemble the first three dynamic modes, and the first EOF mode explains more than 80% of the total variance.

[67] This paper has been influenced by the paper by *Hamilton* [1990] who deployed deep moorings in the gulf, east and west around 25°–26°N and from 1000 to 3000 m. He found highly variable currents in the range, −15 to 15 cm s^{-1}. Whereas the model's deep currents were −5 to 5 cm s^{-1}. Hamilton attributed these deep currents to Topographic Rossby Waves (TRW) and, partially for this reason, we extended the mode calculations to include TRWs; Hamilton worked with approximate TRW formulas and we wished to provide a better theoretical base as summarized by equations (8) and (9). Using rough wave number estimations of l and k provided by Hamilton, our results are in fair agreement with his and correspond to $mH \simeq 0.20$ (see Figure 11b). TRW wave speeds are two to three times LCR speeds and therefore account for the deep waves in Figure 9 at 2500 m, although the signal is quite weak.

[68] Model results show that the mean surface circulation of the Gulf of Mexico is anticyclonic, and suggest that this is mainly due to migrating Loop Current ring. In the deeper layer, the cyclonic circulation occurs along the continental slope. It is suggested that the deep cyclonic circulation in the eastern gulf play an important role in the slope current over the whole gulf as an energy source, which is closely connected to the LC fluctuation.

[69] **Acknowledgments.** We thank T. Ezer and L. Oey for helpful discussion and comments and N. Kim for help with data processing. F. Aikman III and E. Wei provided the Eta data. The authors thanks the referees for their helpful suggestions. The support from NOAA's Geophysical Fluid Dynamics Laboratory and the NOPP funded "Coastal Demonstration Project" are gratefully acknowledged.

References

Aikman, F., III, G. L. Mellor, T. Ezer, D. Sheinin, P. Chen, L. Breaker, K. Bosley, and D. B. Rao, Towards an operational nowcast/forecast system for the U.S. East Coast, in *Modern Approaches to Data Assimilation in Ocean Modeling*, edited by P. Malanotte-Rizzoli, *Elservier Oceanogr. Ser.*, *61*, 347–376, 1996.

Auer, S. J., Five-year climatological survey of the Gulf Stream System and its associated rings, *J. Geophys. Res.*, *92*, 11,709–11,726, 1987.

Blaha, J., and W. Sturges, Evidence for wind-forced circulation in the Gulf of Mexico, *J. Mar. Res.*, *39*, 711–734, 1981.

Blumberg, A. F., and G. L. Mellor, A simulation of the circulation in the Gulf of Mexico, *Isr. J. Earth Sci.*, *34*, 122–144, 1985.

Brooks, D. A., Current and hydrographic variability in the northwestern Gulf of Mexico, *J. Geophys. Res.*, *89*, 8022–8032, 1984.

Chassignet, E. P., and B. Cushman-Roisin, On the influence of a lower layer on the propagation of nonlinear oceanic eddies, *J. Phys. Oceanogr.*, *21*, 939–957, 1991.

Chelton, D. B., and M. G. Schlax, Global observations of oceanic Rossby waves, *Science*, *272*, 234–238, 1996.

Cochrane, J. D., and F. J. Kelly, Low-frequency circulation on the Texas-Louisiana continental shelf, *J. Geophys. Res.*, *91*, 10,645–10,659, 1986.

Elliott, B. A., Anticyclonic rings in the Gulf of Mexico, *J. Phys. Oceanogr.*, *12*, 1292–1309, 1982.

Forristall, G. Z., K. J. Schaudt, and C. K. Cooper, Evolution and kinematics of a Loop Current Eddy in the Gulf of Mexico during 1985, *J. Geophys. Res.*, *97*, 2173–2184, 1992.

Fratantoni, P. S., T. N. Lee, G. P. Podesta, and F. Muller-Karger, The influence of Loop Current perturbations on the formation and elevation of Tortugas eddies in the southern Straits of Florida, *J. Geophys. Res.*, *103*, 24,759–24,779, 1998.

Hamilton, P., Deep current in the Gulf of Mexico, *J. Phys. Oceanogr.*, *20*, 1087–1104, 1990.

Hurlburt, H. E., and D. Thompson, A numerical study of Loop Current intrusions and eddy shedding, *J. Phys. Oceanogr.*, *10*, 1611–1651, 1980.

Johnson, D. R., J. D. Thompson, and J. D. Hawkins, Circulation in the Gulf of Mexico from Geosat altimetry during 1985–1986, *J. Geophys. Res.*, *97*, 2201–2214, 1992.

Kilworth, P. D., D. B. Chelton, and R. A. de Szoeke, The speed of observed and theoretical long extratropical planetary waves, *J. Phys. Oceanogr.*, *27*, 1946–1966, 1997.

Kirwan, A. D., Jr., W. J. Merrell Jr., J. K. Lewis, and R. E. Whitaker, Lagrangian observations of an anticyclonic ring in the western Gulf of Mexico, *J. Geophys. Res.*, *89*, 3417–3424, 1984.

Kundu, P. K., J. S. Allen, and R. L. Smith, Modal decomposition of the velocity filed near the Oregon Coast, *J. Phys. Oceanogr.*, *5*, 683–704, 1975.

LaCasce, J. H., A geostrophic vortex over a slope, *J. Phys. Oceanogr.*, *28*, 2362–2381, 1998.

Lewis, J. K., and A. D. Kirwan Jr., Genesis of a Gulf of Mexico rings as determined from kinematic analyses, *J. Geophys. Res.*, *92*, 11,727–11,740, 1987.

Mellor, G. L., *User's Guide for a Three-Dimensional, Primitive Equation, Numerical Ocean Model*, 41 pp., Prog. in Atmos. and Ocean Sci., Princeton Univ., Princeton, N. J., 1998.

Mellor, G. L., and T. Yamada, Development of a turbulence closure model for geophysical fluid problem, *Rev. Geophys.*, *20*, 851–875, 1982.

Mellor, G. L., C. R. Mechoso, and E. Keto, A diagnostic circulation of the general circulation of the Atlantic Ocean, *Deep Sea Res., Part A*, *29*, 1171–1192, 1982.

Oey, L.-Y., Simulation of mesoscale variability in the Gulf of Mexico: Sensitivity studies, comparison with observations, and trapped wave propagation, *J. Phys. Oceanogr.*, *26*, 145–175, 1996.

Oey, L.-Y., and H.-C. Lee, Deep eddy energy and topographic Rossbby waves in the Gulf of Mexico, *J. Phys. Oceanogr.*, in press, 2002.

Pichevin, T., and D. Nof, The momentum imbalance paradox, *Tellus, Ser. A*, *49*, 298–319, 1997.

Qiu, B., W. Miao, and P. Müller, Propagation and decay of forced and free baroclinic Rossby waves in off-equatorial oceans, *J. Phys. Oceanogr.*, *27*, 2405–2417, 1997.

Richardson, P. L., Gulf Stream trajectories measured with free-drifting buoys, *J. Phys. Oceanogr.*, *11*, 999–1010, 1981.

Smagorinsky, J., S. Manabe, and J. L. Holloway, Numerical results from a nine-level general circulation model of the atmosphere, *Mon. Weather Rev.*, *93*, 727–768, 1965.

Smith, D. C., IV, A numerical study of Loop Current eddy interaction with topography in the western Gulf of Mexico, *J. Phys. Oceanogr.*, *16*, 1260–1272, 1986.

Sturges, W., The spectrum of Loop Current variability from Gappy Data, *J. Phys. Oceanogr.*, *22*, 1245–1256, 1992.

Sturges, W., The annual cycle of the western boundary current in the Gulf of Mexico, *J. Geophys. Res.*, *98*, 18,053–18,068, 1993.

Sturges, W., J. C. Evans, S. Welsh, and W. Holland, Separation of warm core rings in the Gulf of Mexico, *J. Phys. Oceanogr.*, *23*, 250–268, 1993.

Teague, W. J., M. J. Carron, and P. J. Horgan, A comparison between the Generalized Digital Environmental Model and Levitus climatologies, *J. Geophys. Res.*, *95*, 7167–7183, 1990.

Vidal, V. M. V., F. V. Vidal, and J. M. Pérez-Molero, Collision of a Loop Current anticyclonic ring against the continental shelf slope of the western Gulf of Mexico, *J. Geophys. Res.*, *97*, 2155–2172, 1992.

Vidal, V. M. V., F. V. Vidal, E. Meza, J. Portilla, L. Zambrano, and B. Jaimes, Ring-slope interactions and formation of the western boundary current in the Gulf of Mexico, *J. Geophys. Res.*, *104*, 20,523–20,550, 1999.

Vukovich, F. M., An updated evaluation of the Loop Current's eddy-shedding frequency, *J. Geophys. Res.*, *100*, 8655–8659, 1995.

Vukovich, F. M., and B. W. Crissman, Aspects of warm rings in the Gulf of Mexico, *J. Geophys. Res.*, *91*, 2645–2660, 1986.

Welsh, S. E., and M. Inoue, Loop current rings and the deep circulation in the Gulf of Mexico, *J. Geophys. Res.*, *105*, 16,951–16,959, 2000.

Zang, X., and C. Wunsch, The observed dispersion relationship for North Pacific Rossby wave motions, *J. Phys. Oceanogr.*, *29*, 2183–2190, 1999.

H.-C. Lee and G. L. Mellor, AOS Program, Princeton University, P.O. Box Cn710, Princeton, NJ 08644-0710, USA. (lhc@splash.princeton.edu)